

Cite this: *Digital Discovery*, 2024, 3, 2192

Composite machine learning strategy for natural products taxonomical classification and structural insights†

 Qisong Xu,^{ID}^a Alan K. X. Tan,^{ID}^a Liangfeng Guo,^a Yee Hwee Lim,^{ID}^{ab}
 Dillon W. P. Tay,^{ID}^{*a} and Shi Jun Ang,^{ID}^{*acd}

Taxonomical classification of natural products (NPs) can assist in genomic and phylogenetic analysis of source organisms and facilitate streamlining of bioprospecting efforts. Here, a composite machine learning strategy marrying graph convolutional neural networks (GCNNs) and eXtreme Gradient boosting (XGB) is proposed and validated for taxonomical classification of NPs in five kingdoms (Animalia, Bacteria, Chromista, Fungi, and Plantae). Our composite model, trained on 133 092 NPs from the LOTUS database, achieved five-fold cross-validated classification accuracy of 97.4%. When employed to classify out-of-sample NPs from the NP Atlas database, accuracies of 82.8% for bacteria and 86.6% for fungi were obtained. Dimensionality-reduced representations of the molecular embeddings from our composite model revealed distinct clusters of NPs that suggest a basis for enhanced classification performance. The top critical substructures from the NPs of each kingdom were also identified and compared to provide insights on structure–taxonomy relationships. Overall, this study showcases the potential of composite machine learning models for robust taxonomical classification of NPs, which can streamline discovery of NPs.

Received 14th June 2024
Accepted 23rd September 2024

DOI: 10.1039/d4dd00155a

rsc.li/digitaldiscovery

1 Introduction

Natural products (NPs) are synthesized by biological organisms¹ in response to environmental stimuli for their adaptation, interaction, and use in chemical warfare throughout nature.^{2–4} Due to their rich bioactivity, NPs have been employed as agrochemicals,⁵ food preservatives,^{6,7} cosmetics,⁸ and most notably, as pharmaceuticals⁹ where approximately 80% of antibiotics are NP-derived.¹⁰ Recent developments in artificial intelligence (AI) offer unprecedented opportunities to investigate, classify, and characterize NPs.¹¹ Some examples of these include: (1) differentiating between NP and non-NP compounds,¹² (2) classifying terrestrial and marine NPs,¹³ (3) visualizing NP chemical space *via* generative topographic maps,¹⁴ and (4) taxonomically

classifying NPs.^{15,16} In particular, taxonomical classification of NPs can facilitate bioprospecting efforts by providing insights on taxonomic groups producing natural products with interesting bioactivity, thus narrowing investigations to those organisms with shared evolutionary histories.¹⁷ Some examples include: identifying taxonomic groups that produce drug-like molecular scaffolds¹⁸ to guide search efforts for new therapeutic compounds or facilitating the search for natural pesticides¹⁹ and herbicides²⁰ by focusing on plant or microbial species with similar defensive mechanisms. However, current capabilities²¹ only cover three kingdoms (Plantae, Bacteria, and Fungi) which limits the utility of such classifications. Expanding to include more kingdoms would enable more precise and efficient bioprospecting with greater coverage. The convergence of two factors – new advancements in machine learning algorithms²² capable of more effectively tackling this challenge, and the availability of larger curated datasets,²³ makes it an opportune time to undertake this work. Here, we demonstrate a composite machine learning strategy to expand taxonomical classification of NPs to encompass the five kingdoms of Plantae, Bacteria, Fungi, Animalia, and Chromista²⁴ (Fig. 1).

Graph convolutional neural networks (GCNNs)^{22,27,28} are first employed to effectively extract key structural features of NPs as molecular fingerprints that are then used as the input for traditional machine learning algorithms²⁹ like Support Vector Machines (SVMs)³⁰ or eXtreme Gradient Boosting (XGB).³¹ The combination of molecular fingerprints generated by GCNNs

^aInstitute of Sustainability for Chemicals, Energy and Environment (ISCE²), Agency for Science, Technology and Research (A*STAR), 8 Biomedical Grove, #07-01 Neuros Building, Singapore 138665, Republic of Singapore. E-mail: dillon_tay@isce2.a-star.edu.sg

^bSynthetic Biology Translational Research Program, Yong Loo Lin School of Medicine, National University of Singapore, Singapore 117597, Republic of Singapore

^cInstitute of High Performance Computing (IHPC), Agency for Science, Technology and Research (A*STAR), 1 Fusionopolis Way, #16-16 Connexis, Singapore 138632, Republic of Singapore. E-mail: ang_shi_jun@ihpc.a-star.edu.sg

^dDepartment of Chemistry, National University of Singapore, 3 Science Drive 3, Singapore 117543, Republic of Singapore

† Electronic supplementary information (ESI) available. See DOI: <https://doi.org/10.1039/d4dd00155a>



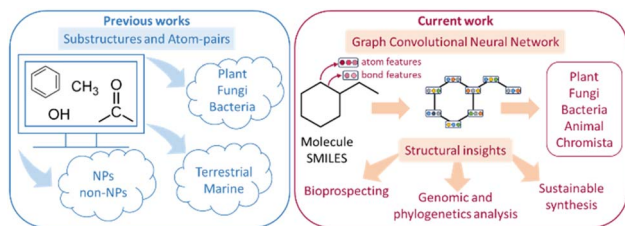


Fig. 1 Previous studies^{12,13,21,25,26} have focused on substructure and atom-pair information to predict up to three natural product (NP) kingdoms. In this work, composite machine learning models are developed to taxonomically classify NPs in up to five different kingdoms.

and XGB yielded the most robust classification models (97.4% balanced accuracy), providing improvements of ~15% in balanced accuracy over incumbent model architectures.²¹ Our composite models could also be used to characterize complex molecular targets³² or molecules crafted through generative chemistry.³³

2 Materials and methods

2.1 Dataset preparation

An open-source and well-annotated database of natural products from the LOTUS initiative was utilized.²³ This involved an original dataset (LOTUS version from February 2021) consisting of 276 518 NPs retrieved from the official LOTUS website (<https://lotus.naturalproducts.net/download>). The SMILES (Simplified Molecular Input Line Entry System)³⁴ of NPs were first canonicalized, giving rise to 276 499 unique isomeric

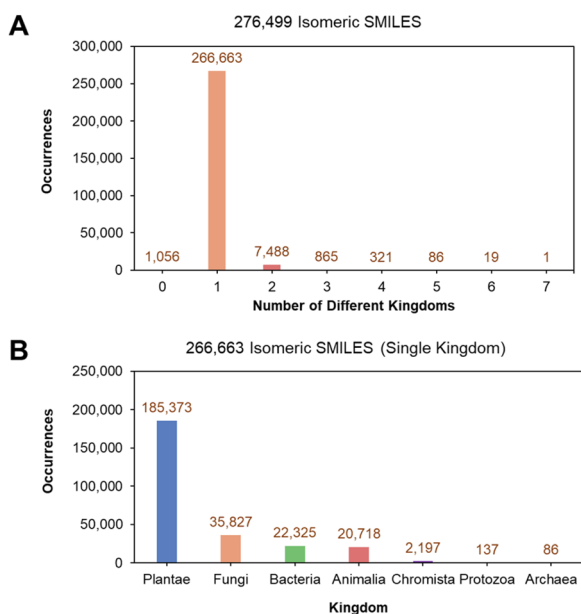


Fig. 2 Distribution of isomeric SMILES in the LOTUS database. (A) Distribution of isomeric SMILES by number of kingdoms, and (B) kingdom distribution of isomeric SMILES belonging to only a single kingdom.

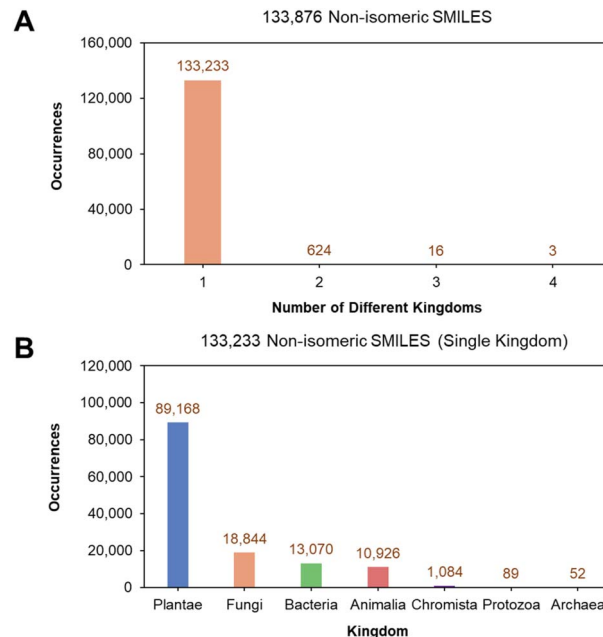


Fig. 3 Distribution of non-isomeric SMILES in the LOTUS database. (A) Distribution of non-isomeric SMILES by number of kingdoms and (B) kingdom distribution of non-isomeric SMILES belonging to only a single kingdom.

SMILES that illustrate the diversity of NPs with varying stereochemistry. Seven kingdoms were identified from the annotations of the original LOTUS dataset: Animalia, Archaea, Bacteria, Chromista, Fungi, Plantae, and Protozoa. 266 663 isomeric SMILES (96.44% of the original 276 499 isomeric SMILES) only held a single kingdom label (Fig. 2A). A detailed breakdown of the 266 663 single kingdom isomeric SMILES showed that the largest population of characterized NPs originated from Plantae, followed by Fungi, Bacteria, and Animalia kingdoms (Fig. 2B).

Removing isomeric information from the 266 663 single kingdom isomeric SMILES reduced them to 133 876 unique non-isomeric SMILES (Fig. 3A) of which 133 233 (99.52% out of 133 876) hold single-kingdom labels. This suggests that despite the presence of stereochemistry, different stereoisomers of the same non-isomeric SMILES originate mostly from the same kingdom. Similarly, the kingdom distribution for the 133 233 non-isomeric SMILES is also dominated by NPs from the Plantae kingdom (Fig. 3B). The final curated dataset for multi-class classification and structural analysis comprised of SMILES from the top five kingdoms (Animalia, Bacteria, Chromista, Fungi, and Plantae), totalling 133 092 unique non-isomeric entries, as the kingdoms of Protozoa and Archaea each contributed less than 1% to the dataset.

Subsequent machine learning models were trained on these 133 092 unique, single kingdom label, non-isomeric SMILES for multiclass classification to five kingdoms (Animalia, Bacteria, Chromista, Fungi, and Plantae). It is important to note the limitation that models trained on this non-isomeric SMILES dataset do not consider chirality information when performing taxonomical classification. Addressing this limitation and incorporating



chirality and multiple kingdom labels into future models represents a possible avenue for further research, potentially further enhancing the accuracy of NP taxonomical classification.

2.2 Multiclass classification

A two-step composite method of machine learning algorithms was considered for multiclass classification. First, a GCNN approach employing directed message-passing neural networks (D-MPNN) and feed-forward neural network (FFNN) where non-isomeric NP SMILES were utilized as inputs (Fig. 4).²⁸ The D-MPNN consists of a message passing phase that transmits atomic and bond features to construct the molecular embedding of an NP, followed by a readout phase of the molecular embedding *via* FFNN to predict its kingdom category.²² Additionally, the use of seven different machine learning (ML) classifiers were also investigated using three types of fingerprints, namely, MAP4 fingerprints,²⁵ MPN fingerprints (from D-MPNN) and last_FFNN fingerprints (from the last layer of the FFNN) to develop composite ML models. MPN and last_FFNN fingerprints were derived from a GCNN model trained on the entire curated dataset (133 092 non-isomeric SMILES). The dimension of the MAP4 fingerprints was 1,024, while both MPN and last_FFNN fingerprints have dimensions of 1,100, which is the default in *Chemprop*. The seven ML classifier algorithms explored include Gaussian Naive Bayes (NB), K-Nearest Neighbors (KNN), Quadratic Discriminant Analysis (QDA), Random Forest (RF), Light Gradient Boosting Machine (LGBM), eXtreme Gradient Boosting (XGB), and Support Vector Machine (SVM) with linear kernel. The hyperparameters of the GCNN models were optimized and the molecular fingerprints calculated using the respective `chemprop.hyperparameter_optimization` and `chemprop.fingerprint` objects from the *Chemprop* package.²⁸ During the optimization of the GCNN models, a total of 200 epochs with batch size of 50 were found to be sufficient. On the other hand, the seven ML models were trained using the *scikit-learn* package.²⁹ For all learning algorithms, a five-fold cross validation *via* stratified sampling of the five kingdoms was implemented to evaluate the multiclass classification performance of the training and validation set. The performance of all multiclass classification models were evaluated by balanced accuracy, Matthews correlation coefficient (MCC), and F1 score. The mean and standard errors of the metrics from five-fold cross validation were also used to compare the classification performance. The classification metrics were calculated based on the counts of true positive (TP), false positive (FP), true negative (TN), false negative (FN), as follows:

$$\text{Balanced accuracy} = \frac{\frac{TP}{TP + FP} + \frac{TN}{TN + FN}}{2}$$

$$\text{Accuracy} = \frac{TP + TN}{TP + TN + FP + FN}$$

$$\text{Matthews correlation coefficient (MCC)} = \frac{TP \times TN - FP \times FN}{\sqrt{(TP + FP)(TP + FN)(TN + FP)(TN + FN)}}$$

$$\text{Precision} = \frac{TP}{TP + FP}$$

$$\text{Recall} = \frac{TP}{TP + FN}$$

$$\text{F1 score} = 2 \times \frac{(\text{Precision} \times \text{Recall})}{(\text{Precision} + \text{Recall})}$$

2.3 Structural analysis

In addition to optimizing multiclass classification models, the molecular embeddings were also analyzed to verify the validity of the trained models. After five-fold cross validation of all models, a final GCNN model was trained using the full dataset of 133 092 non-isomeric SMILES. Through *t*-distributed stochastic neighbor embedding (*t*-SNE), the high-dimensional MAP4 fingerprints as well as MPN and last_FFNN fingerprints from the final GCNN model were dimensionally reduced and elucidated. A series of four different perplexity parameters [10^2 , 10^3 , 10^4 and 10^5] were explored to ensure impartiality when visualizing the two-dimensional (2D) projection clustering of NPs from different kingdoms. To evaluate the performance of *t*-SNE for different perplexity values, the Kullback–Leibler (KL) divergence between the original and fitted distribution of molecular fingerprints was assessed while the separation among clusters was quantified by Davies–Bouldin (DB) score. Molecular embeddings and their evaluation were performed using the *t*-SNE and DB_score objects in *scikit-learn* package.²⁹

Finally, we analyzed the substructures of the NP molecules to identify critical structural fragments and their combinations that are characteristic of their kingdom source. The Monte Carlo Tree Search was employed to determine critical substructures using the `chemprop.interpret` object in *Chemprop* package.²⁸ By analyzing the Bemis–Murcko scaffolds of NPs,³⁵ the top critical scaffolds from each kingdom were identified.³⁶

3 Results and discussion

A GCNN model was trained on the curated 133 092 non-isomeric SMILES dataset to perform taxonomical classification of NPs from their structures. Subsequently, different ML models and molecular fingerprints were investigated to evaluate

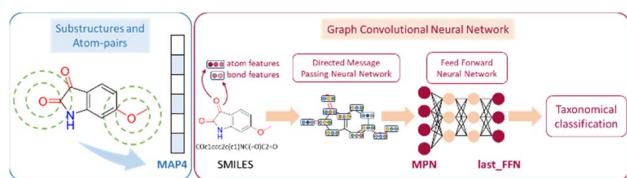


Fig. 4 Using the molecular structure of 6-methoxyisatin as an example, the generated MAP4, MPN and last_FFNN fingerprints are illustrated.^{22,25}



their influence on multiclass classification performance. To assess the transferability of the developed classification models, the best models were applied to NP taxonomical classification beyond the training set. Finally, we structurally analyzed NPs through dimensionally reduced molecular embeddings to identify and compare critical substructures of NPs in each kingdom.

3.1 Multiclass classification

3.1.1 Overall classification performance. The overall classification performance of the different algorithms is compared in terms of balanced accuracy and MCC (see Table S1† for training results and Table 1 for validation results). The GCNN model trained to classify NPs into five different kingdoms gave a balanced accuracy of 85.6% and MCC of 87.3% on the validation set. Comparatively, the literature SVM model architecture using MAP4 fingerprints trained on the 133 092 non-isomeric SMILES dataset gave a slightly poorer balanced accuracy of 82.2% and MCC of 87.0% for the validation set.²¹ Pursuing further improvement, we explored additional ML models to supplement the prediction capabilities of simple GCNN models for more accurate taxonomical classification.

Seven ML algorithms (NB, QDA, KNN, RF, LGBM, XGB, and SVM) based on three different types of fingerprints (MAP4, MPN, and last_FFN) were further explored as a composite strategy to supplement GCNN classification capability (Tables 1 and S1†). Classification models developed from MPN and last_FFN fingerprints provided better classification performance than those constructed from MAP4 fingerprints. This is evident from the high balanced accuracy and MCC in training and validation for all algorithms using MPN and last_FFN fingerprints. Unlike MAP4 fingerprints that comprise of circular substructure and atom-pair information,²⁵ both MPN and last_FFN fingerprints are based on more detailed, information-rich graph representations of NPs suitable for accurate classification (Fig. 4). Furthermore, ML models based on last_FFN fingerprints offer the best classification performance that could potentially be attributed to its feed-forward neural network that

facilitates additional learning drawn from MPN molecular embeddings.²²

The classification performance of NPs also depended on the nature of the ML algorithm. For all three types of fingerprints, classification models based on NB and QDA generally performed poorly, as observed from their low accuracies and MCC scores (Tables S1† and 1). This may be due to the probabilistic nature of NB and QDA, which is sensitive to the kingdom populations and skew higher probabilities toward the major class.^{37,38} For KNN, the balanced accuracy and MCC improved for all three fingerprints, together with comparable classification performance for both training and validation sets. RF and SVM are two high-performing models that provided significant improvements in both classification accuracy and precision. This is because RF combines results from multiple trees to describe complex decision boundaries,³⁹ while SVM is resilient to outliers by identifying optimal hyperplanes that maximize class separation.³⁰ Finally, ensemble learning strategies involving tree-based models such as LGBM⁴⁰ and XGB³¹ demonstrated good performance, in-line with their ability to handle imbalanced classes well and prevent overfitting with regularization. To this end, the prediction performance of the GCNN-XGB composite model developed based on last_FFN fingerprints significantly outperformed those from simple GCNN models and the MAP4-SVM model from previous studies (Fig. 5).²¹

3.1.2 Classification performance for each kingdom.

Balanced accuracies and F1 scores from the GCNN model ranged between 80%-90% for each kingdom (Fig. S4†). This performance was comparable to those of previous studies for bacteria (89%), fungi (89%) and plants (94%).²¹ It is also noteworthy that the variation in classification performance for each kingdom generally increases from Chromista to Plantae, mirroring the order of increasing NP populations from chromists to plants present in the curated dataset. This trend reinforces the importance of data quantity to enhance machine learning model performance to provide more accurate assignments of kingdom origins.

In addition, the influence of traditional ML algorithms and molecular fingerprints on individual classification performance

Table 1 Comparison of Balanced Accuracy (BA) and MCC of simple GCNN *versus* composite models to predict five different kingdoms (Animalia, Bacteria, Chromista, Fungi, and Plantae) using different molecular fingerprints and machine learning algorithms. Values reported are validation set results from stratified 5-fold cross validation^a

Algorithm	MAP4		GCNN-MPN		GCNN-last_FFN	
	BA	MCC	BA	MCC	BA	MCC
GCNN	—	—	—	—	85.6 ± 0.8	87.3 ± 0.5
NB	20.0 ± 0.0	0.0 ± 0.0	30.8 ± 0.4	39.0 ± 0.7	67.5 ± 0.8	83.9 ± 0.5
QDA	29.4 ± 0.1	12.8 ± 0.4	63.1 ± 0.3	79.6 ± 0.4	96.5 ± 0.4	96.5 ± 0.1
KNN	54.5 ± 4.5	59.8 ± 4.4	82.5 ± 0.9	87.0 ± 0.6	93.9 ± 0.6	96.8 ± 0.1
RF	58.1 ± 0.9	67.6 ± 0.2	84.8 ± 0.9	91.5 ± 0.3	96.8 ± 0.5	97.8 ± 0.1
LGBM	68.3 ± 0.8	72.5 ± 0.3	90.2 ± 0.8	93.5 ± 0.2	97.2 ± 0.3	97.9 ± 0.1
XGB	72.1 ± 0.9	76.7 ± 0.3	91.1 ± 0.6	93.8 ± 0.1	97.4 ± 0.2	97.9 ± 0.1
SVM	82.2 ± 0.5	87.0 ± 0.3	90.9 ± 0.5	92.4 ± 0.2	97.1 ± 0.3	97.9 ± 0.1

^a BA = Balanced Accuracy. MCC = Matthews Correlation Coefficient. GCNN = Graph Convolutional Neural Network. NB = Gaussian Naïve Bayesian. QDA = Quadratic Discriminant Analysis. RF = Random Forest. SVM = Support Vector Machine. LGBM = Light Gradient-Boosting Machine. XGB = eXtreme Gradient Boosting. Error of 1 standard deviation shown.



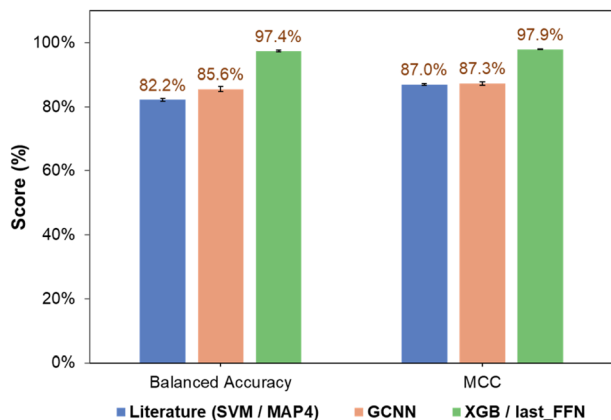


Fig. 5 Comparison of overall performance of SVM classification model using MAP4 fingerprints from Capecchi and Raymond²¹ and current work (GCNN and GCNN-SVM developed using last_FFNN fingerprints).

for each kingdom is reported in detail (Fig. S5–S10[†]). High accuracies and F1 scores were observed for each kingdom when ML models were constructed with MPN and last_FFNN fingerprints, demonstrating the advantages of MPN and last_FFNN fingerprints over MAP4 fingerprints. In terms of ML algorithms, NB and QDA models performed poorly in classification (low accuracy and F1 score) for most kingdoms. The classification accuracies and F1 scores decrease from Plantae to Chromista, again mirroring their population sizes in the dataset. On the other hand, SVM³⁰ classified accurately for each kingdom despite the differences in kingdom populations. This is because SVMs provide multiple class separation despite the difference in occurrences. RF³⁹ demonstrated excellent training classification performance across different kingdoms due to its ability to handle complex, high-dimensional data. Finally, ensemble learning strategies involving tree-based models such as LGBM⁴⁰ and XGB³¹ also performed well due to their leaf-wise growth strategy focusing on the most significant splits and in-built regularization respectively. Overall, the composite strategy of layering XGB on top of last_FFNN fingerprints provided the best classification model for the accurate taxonomical classification of NPs.

3.1.3 Database screening. To evaluate the transferability of trained models, we further employed the pre-trained GCNN, SVM, and composite models to screen the NP Atlas database

(NP Atlas v2023_06 from <https://www.npatlas.org/download>).⁴¹ The NP Atlas database consists of NPs that originate from the kingdoms of Bacteria and Fungi. Out of the 33 372 NPs present, 13 136 NPs (7446 from Bacteria and 5690 from Fungi) are not found in the LOTUS database used for training our models. GCNN-SVM, GCNN-LGBM, and GCNN-XGB composite models with comparable performance were evaluated on the NP Atlas test set.

The composite GCNN-XGB model performed markedly better at classification compared to simple GCNN and composite GCNN-MPN models (Table 2). However, it trades bacterial NP classification accuracy for fungal NP accuracy when compared to the literature benchmark SVM model using MAP4 molecular fingerprints.

3.2 Structural analysis of NPs

To verify the remarkable classification performance of the developed GCNN and composite ML models, structural analyses of MAP4, MPN and last_FFNN fingerprints were performed through the *t*-SNE dimensionality reduction algorithm. Kullback–Leibler (KL) divergence values for each of the molecular fingerprints decrease with perplexity value (Fig. S11a[†]). For all explored perplexity values however, last_FFNN fingerprints possessed the lowest Davies–Bouldin (DB) score amongst all other fingerprints (Fig. S11b[†]) and provided the most distinct kingdom clusters. Using the perplexity value of 10^4 as a comparison, MAP4 fingerprints displayed NPs with highly overlapping structural features (Fig. 6A), which led to the poor classification performance observed in the previous section. On the other hand, MPN fingerprints exhibited substantial separation in the molecular features of NPs from different kingdoms (Fig. 6B), as the MPN fingerprints describe the structural similarity of NPs based on its chemical graph representation. Employing FFNNs to extract additional learning from MPN fingerprints yielded last_FFNN fingerprints that facilitated the best NP taxonomical classification with well-separated clusters of NPs belonging to their respective kingdoms (Fig. 6C).

Next, the critical substructures in NPs contributing to the classification of kingdom origins were determined. A Monte Carlo Tree Search (MCTS) was used to identify critical chemical fragments in the molecular structures of NPs. The top ten critical substructures deemed by the trained GCNN model as the most informative for NP taxonomical classification are listed for

Table 2 Comparison of classification performance for 13 136 NP Atlas test set

Model	Molecular fingerprint	Bacterial NP accuracy (%)	Fungal NP accuracy (%)
SVM	MAP4	89.9	81.6
GCNN	last_FFNN	81.1	86.0
GCNN-SVM	MPN	80.2	82.9
GCNN-SVM	last_FFNN	83.2	86.5
GCNN-LGBM	MPN	82.7	82.9
GCNN-LGBM	last_FFNN	82.7	86.3
GCNN-XGB	MPN	84.0	82.6
GCNN-XGB	last_FFNN	82.8	86.6



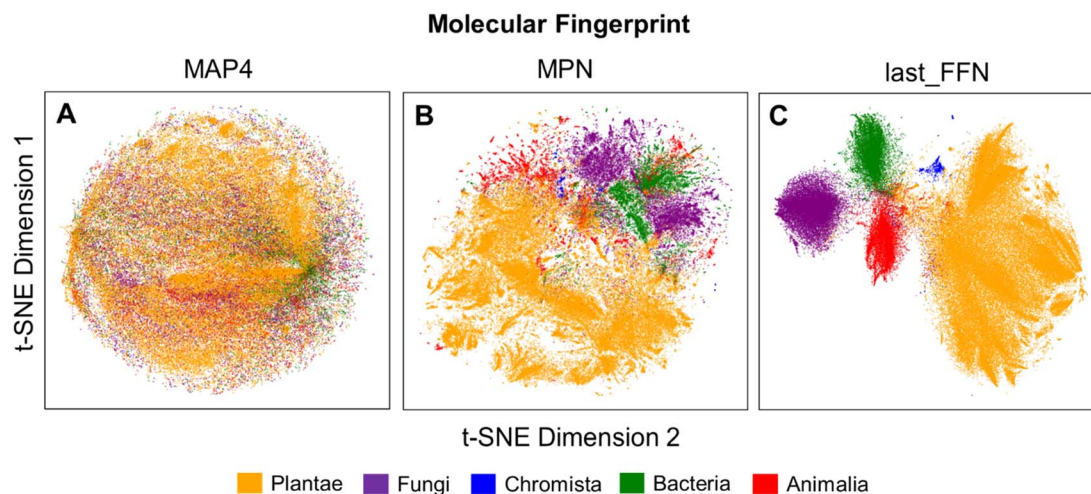


Fig. 6 Visualization of the 2D projection using *t*-SNE (perplexity value of 10^4) using (A) MAP4, (B) MPN and (C) last_FFN fingerprints from the final trained GCNN model.

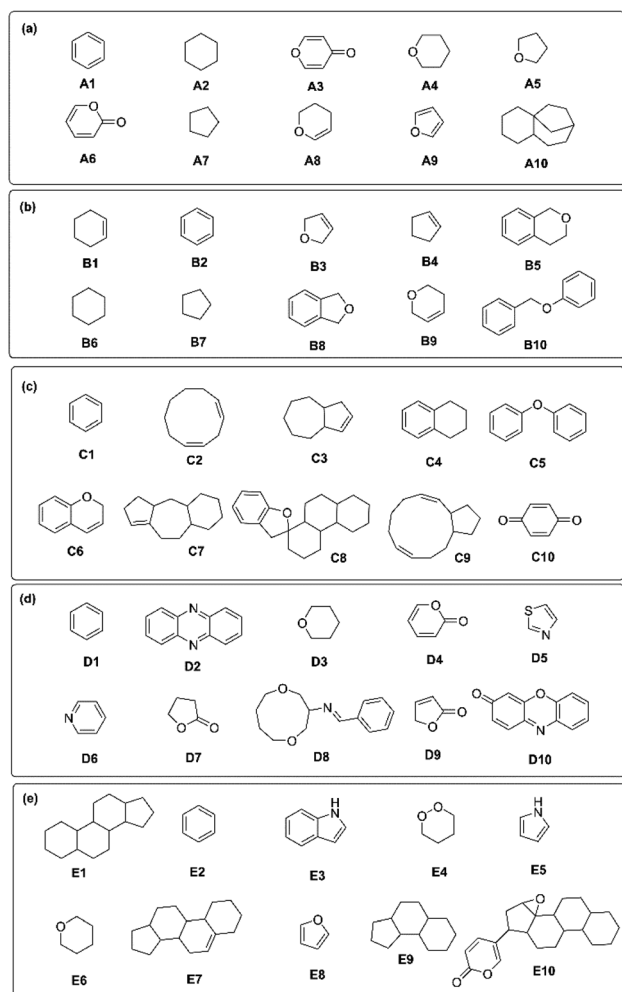


Fig. 7 Combinations of critical substructures identified in the five kingdoms of (A) Plantae, (B) Fungi (C) Chromista, (D) Bacteria, and (E) Animalia.

each kingdom (Fig. 7). Critical chemical substructures were identified as possessing a rationale score of more than 0.8, calculated from the chemprop.interpret object in *Chemprop* package.²⁸

Interestingly, the identified NP scaffolds also share structural similarities with essential starting fragments for drug discovery.⁴² The critical substructures for NPs in Plantae, Fungi and Chromista mainly consist of oxygen-based heterocycles (Fig. 7A–C). For plant NPs, the critical substructures tend to be simpler in nature, including furan-like⁴³ (A5, A9), pyran-like⁴⁴ (A3, A4, A8), and lactones⁴⁵ (A6). In fungal NPs, molecular systems of fused rings (B5, B8) and linked rings (B10) were found to be critical. For chromists, the critical substructures identified in their NPs tended toward more complex fused ring systems (C3, C7, C8) and macrocycles (C2, C9). On the other hand, bacterial NPs typically consist of nitrogen-based heterocycles,⁴⁶ including pyridine (D6), thiazole (D5), phenazine (D2) and phenoxazine-like moieties (D10) (Fig. 7D), with a few critical lactone fragments also identified (D4, D7, D9). Nitrogen-fused heterocycles such as pyrrole (E5) and indole (E3) were found to be important for critical substructures in animal NPs (Fig. 7E),⁴⁷ on top of three- (E9) and four-fused (E1, E7, E9) ring systems resembling steroids.⁴⁸ The benzene ring is a highly common and critical substructure across all five kingdoms (A1, B2, C1, D1 and E2). Owing to the high structural stability conferred by resonance, the planar aromatic rings offer stable building blocks that are ubiquitously found in nature. As fragments such as benzene and furan (A9, E8) are shared between kingdoms, individual fragments cannot inform taxonomical classification. Instead, it is the unique combination and connectivity of these fragments that drive differentiation between kingdoms. This underscores the importance of analyzing the broader structural context of NP structures *via* the right molecular fingerprinting technique rather than relying solely on the presence of individual substructures. All of the substructures described above are critical to the synthesis of stable NPs with differing levels of structural complexity.^{2,49}



Structural analyses such as these provide valuable insights into the key fragments and potential fragment combinations characteristic of each kingdom, supporting *in silico* bioprospecting efforts to systematically identify the biochemical origins of novel NPs.¹⁷ Furthermore, the identified relationships between critical fragments and the corresponding kingdoms from which the NPs originate can prompt future genomic and phylogenetic analyses of different organisms to reveal the fundamental biosynthesis pathways of NPs occurring in nature.⁵⁰ Overall, by leveraging on GCNNs, the structural features of NPs are effectively captured through molecular graphs, facilitating the formation of well-separated clusters corresponding to the five kingdoms. Identifying these critical substructures also enhances the explainability and interpretability of our composite machine learning models, offering a clearer understanding of how they utilize structural information for taxonomical classification.

4 Conclusion

Using a composite machine learning strategy, we optimized a multiclass classification model for taxonomical classification of NPs from their structures. By analyzing the LOTUS database, we determined the kingdom-specific critical substructures of NPs for five kingdoms (Animalia, Bacteria, Chromista, Fungi, and Plantae). GCNN models trained on 133 092 non-isomeric SMILES across these five kingdoms were found to classify with a slightly superior performance to those of previous studies. Notably, the classification performance within each kingdom were found to increase with NP populations (*i.e.* data quantity). Three types of molecular fingerprints (MAP4, MPN, and last_FFN) were explored using seven different ML algorithms (NB, KNN, QDA, RF, LGBM, XGB, and SVM). The composite GCNN-XGB model merging last_FFN fingerprints with XGB yielded the best classification performance of 97.4% balanced accuracy on the validation set. When extended to classifying NPs outside of the training set from the NP Atlas database, the composite GCNN-XGB model achieved accuracies of 82.8% for Bacteria and 86.6% for Fungi. *t*-SNE embeddings of the three different molecular fingerprints revealed that last_FFN fingerprints gave the most well-separated clusters of NPs that resulted in remarkable classification performance. Finally, the top critical substructures characteristic for NPs in each kingdom were identified and compared to provide insights to structure–taxonomy relationships. Overall, this study demonstrates the potential of a composite machine learning strategy for taxonomically classifying NPs and to provide structural insights. Adopting this approach not only accelerates the classification of NP origins to screen for novel bioactive candidates but can also highlight kingdom-unique structural features of NPs to guide future efforts in virtual screening for bioprospecting as well as genomic and phylogenetic analyses of different organisms. Future avenues to enhance taxonomy classification include adopting advanced strategies such as hybrid data-based learning,⁵¹ multi-level learning,⁵² or meta-learning⁵³ to further extend the generalizability of trained

models across various dimensions, such as molecular size, functional groups, and structural complexity.

Code availability

The code used to train and evaluate composite models for taxonomical classification of natural products is available from GitHub at <https://github.com/SIBERanalytics/NPTaxonomy>.

Data availability

The dataset used in this work to develop taxonomical classification of NPs was acquired from the LOTUS initiative (<https://lotus.naturalproducts.net/download>).²³ Processed LOTUS SMILES dataset,⁵⁴ MPN and last_FFN fingerprints⁵⁵ are available in (.csv) format on figshare. The screening dataset was obtained from the NP Atlas database (NP Atlas v2023_06 from <https://www.npatlas.org/download>).⁴¹ Processed NP Atlas MPN fingerprints, and last_FFN fingerprints⁵⁶ available in (.csv) format on figshare. Deep learning of NPs and Monte Carlo Tree Search were performed using the *Chemprop* package in python.²⁸ The machine learning of fingerprints, calculation of *t*-distributed stochastic neighbor embedding, Kullback–Leibler divergence and Davies–Bouldin score were achieved using the *scikit-learn* package in python.²⁹ Pre-trained composite GCNN-SVM (MPN fingerprints)⁵⁷ and GCNN-SVM (last_FFN fingerprints)⁵⁸ classification models for NP taxonomical classification can be downloaded from figshare. Pre-trained composite GCNN-LGBM and GCNN-XGB classification models using both MPN and last_FFN fingerprints are available from GitHub at <https://github.com/SIBERanalytics/NPTaxonomy>.

Author contributions

S. J. A. conceptualized, designed, and supervised the study. Y. H. L. acquired funding and conceptualized the study. D. W. P. T. supervised the study. The following authors conducted the investigation and performed data analysis: Q. X., A. K. X. T., L. G., and D. W. P. T. Data curation was done by Q. X. Data visualization was performed by Q. X. and D. W. P. T. Q. X. wrote the manuscript with inputs from all authors. All authors participated in reviewing and editing the manuscript.

Conflicts of interest

The authors declare no conflicts of interest.

Acknowledgements

The authors gratefully acknowledge financial support from the Agency for Science, Technology and Research (A*STAR), Singapore (C233017006) for this work. Q. Xu thanks National Research Foundation Singapore for the funding through SGUnited Jobs Initiative (P20J3d1014). This work was supported by A*STAR Computational Resource Centre and the National



Supercomputing Centre, Singapore (<https://www.nsc.sg>) through the use of their high performance computing facilities.

Notes and references

- D. J. Newman and G. M. Cragg, *J. Nat. Prod.*, 2020, **83**, 770–803.
- M. Grigalunas, S. Brakmann and H. Waldmann, *J. Am. Chem. Soc.*, 2022, **144**, 3314–3329.
- Y.-M. Shi and H. B. Bode, *Nat. Prod. Rep.*, 2018, **35**, 309–335.
- S. Wöll, S. H. Kim, H. J. Greten and T. Efferth, *Nat. Prod. Bioprospect.*, 2013, **3**, 1–7.
- T. C. Sparks, D. R. Hahn and N. V. Garizi, *Pest Manag. Sci.*, 2017, **73**, 700–715.
- S. González-Manzano and M. Dueñas, *Foods*, 2021, **10**(2), 300.
- S. C. Lourenço, M. Moldão-Martins and V. D. J. M. Alves, *Molecules*, 2019, **24**, 4132.
- J. B. Sharmeen, F. M. Mahomoodally, G. Zengin and F. Maggi, *Molecules*, 2021, **26**(3), 666.
- F. E. Koehn and G. T. Carter, *Nat. Rev. Drug Discovery*, 2005, **4**, 206–220.
- D. J. Newman and G. M. Cragg, *J. Nat. Prod.*, 2016, **79**, 629–661.
- M. W. Mullowney, K. R. Duncan, S. S. Elsayed, N. Garg, J. J. J. van der Hooft, N. I. Martin, D. Meijer, B. R. Terlouw, F. Biermann, K. Blin, J. Durairaj, M. Gorostiola González, E. J. N. Helfrich, F. Huber, S. Leopold-Messer, K. Rajan, T. de Rond, J. A. van Santen, M. Sorokina, M. J. Balunas, M. A. Beniddir, D. A. van Bergeijk, L. M. Carroll, C. M. Clark, D.-A. Clevert, C. A. Dejong, C. Du, S. Ferrinho, F. Grisoni, A. Hofstetter, W. Jespers, O. V. Kalinina, S. A. Kautsar, H. Kim, T. F. Leao, J. Masschelein, E. R. Rees, R. Reher, D. Reker, P. Schwaller, M. Segler, M. A. Skinnider, A. S. Walker, E. L. Willighagen, B. Zdrzil, N. Ziemert, R. J. M. Goss, P. Guyomard, A. Volkamer, W. H. Gerwick, H. U. Kim, R. Müller, G. P. van Wezel, G. J. P. van Westen, A. K. H. Hirsch, R. G. Linington, S. L. Robinson and M. H. Medema, *Nat. Rev. Drug Discovery*, 2023, **22**, 895–916.
- P. Ertl, S. Roggo and A. Schuffenhauer, *J. Chem. Inf. Model.*, 2008, **48**, 68–74.
- F. Pereira, *Mol. Inform.*, 2021, **40**, 2060034.
- Y. Zabolotna, P. Ertl, D. Horvath, F. Bonachera, G. Marcou and A. Varnek, *Mol. Inform.*, 2021, **40**, 2100068.
- Y. Djoumbou Feunang, R. Eisner, C. Knox, L. Chepelev, J. Hastings, G. Owen, E. Fahy, C. Steinbeck, S. Subramanian, E. Bolton, R. Greiner and D. S. Wishart, *J. Cheminf.*, 2016, **8**, 61.
- H. W. Kim, M. Wang, C. A. Leber, L.-F. Nothias, R. Reher, K. B. Kang, J. J. J. van der Hooft, P. C. Dorrestein, W. H. Gerwick and G. W. Cottrell, *J. Nat. Prod.*, 2021, **84**, 2795–2807.
- K. Santana, L. D. do Nascimento, A. Lima e Lima, V. Damasceno, C. Nahum, R. C. Braga and J. Lameira, *Front. Chem.*, 2021, **9**, 662688.
- F. Zhu, C. Qin, L. Tao, X. Liu, Z. Shi, X. Ma, J. Jia, Y. Tan, C. Cui, J. Lin, C. Tan, Y. Jiang and Y. Chen, *Proc. Natl. Acad. Sci. U.S.A.*, 2011, **108**, 12943–12948.
- A. L. Hans and S. Saxena, in *Bioprospecting of Plant Biodiversity for Industrial Molecules*, 2021, pp. 335–344, DOI: [10.1002/9781119718017.ch16](https://doi.org/10.1002/9781119718017.ch16).
- D. Schein, M. S. N. Santos, S. Schmaltz, L. E. P. Nicola, C. F. Bianchin, R. G. Ninaus, B. B. d. Menezes, R. C. d. Santos, G. L. Zabot, M. V. Tres and M. A. Mazutti, *Processes*, 2022, **10**, 2001.
- A. Capecchi and J.-L. Reymond, *J. Cheminf.*, 2021, **13**, 82.
- E. Heid, K. P. Greenman, Y. Chung, S.-C. Li, D. E. Graff, F. H. Vermeire, H. Wu, W. H. Green and C. J. McGill, *J. Chem. Inf. Model.*, 2024, **64**, 9–17.
- A. Rutz, M. Sorokina, J. Galgonek, D. Mietchen, E. Willighagen, A. Gaudry, J. G. Graham, R. Stephan, R. Page, J. Vondrášek, C. Steinbeck, G. F. Pauli, J.-L. Wolfender, J. Bisson and P.-M. Allard, *eLife*, 2022, **11**, e70780.
- T. Cavalier-Smith, *Biol. Lett.*, 2009, **6**, 342–345.
- A. Capecchi, D. Probst and J.-L. Reymond, *J. Cheminf.*, 2020, **12**, 43.
- A. Capecchi and J.-L. Reymond, *Biomolecules*, 2020, **10**.
- J. Gilmer, S. S. Schoenholz, P. F. Riley, O. Vinyals and G. E. Dahl, *ICML*, 2017, pp. 1263–1272.
- K. Yang, K. Swanson, W. Jin, C. Coley, P. Eiden, H. Gao, A. Guzman-Perez, T. Hopper, B. Kelley, M. Mathea, A. Palmer, V. Settels, T. Jaakkola, K. Jensen and R. Barzilay, *J. Chem. Inf. Model.*, 2019, **59**, 3370–3388.
- F. Pedregosa, G. Varoquaux, A. Gramfort, V. Michel, B. Thirion, O. Grisel, M. Blondel, P. Prettenhofer, R. Weiss and V. Dubourg, *J. Mach. Learn. Res.*, 2011, **12**, 2825–2830.
- C. Cortes and V. Vapnik, *Mach. Learn.*, 1995, **20**, 273–297.
- T. Chen and C. Guestrin, presented in part at the *Proceedings of the 22nd ACM SIGKDD International Conference on Knowledge Discovery and Data Mining*, San Francisco, California, USA, 2016.
- F. Hemmerling and J. Piel, *Nat. Rev. Drug Discovery*, 2022, **21**, 359–378.
- D. W. P. Tay, N. Z. X. Yeo, K. Adaikkappan, Y. H. Lim and S. J. Ang, *Sci. Data*, 2023, **10**, 296.
- D. Weininger, *J. Chem. Inf. Comput. Sci.*, 1988, **28**, 31–36.
- G. W. Bemis and M. A. Murcko, *J. Med. Chem.*, 1996, **39**, 2887–2893.
- Y. Chen, C. Rosenkranz, S. Hirte and J. Kirchmair, *Nat. Prod. Rep.*, 2022, **39**, 1544–1556.
- H. Zhang, *Proc. Seventeenth Int. Florida Artif. Intell. Res. Soc. Conf.*, 2004, **1**, 562–567.
- T. Hastie, R. Tibshirani and J. Friedman, *The elements of statistical learning: data mining, inference, and prediction*, Springer Science & Business Media, 2009.
- L. Breiman, *Mach. Learn.*, 2001, **45**, 5–32.
- G. Ke, Q. Meng, T. Finley, T. Wang, W. Chen, W. Ma, Q. Ye and T.-Y. Liu, presented in part at the *Proceedings of the 31st International Conference on Neural Information Processing Systems*, Long Beach, California, USA, 2017.



- 41 J. A. van Santen, E. F. Poynton, D. Iskakova, E. McMann, T. A. Alsup, T. N. Clark, C. H. Fergusson, D. P. Fewer, A. H. Hughes, C. A. McCadden, J. Parra, S. Soldatou, J. D. Rudolf, E. M. L. Janssen, K. R. Duncan and R. G. Linington, *Nucleic Acids Res.*, 2022, **50**, D1317–D1323.
- 42 S. F. Martin, *J. Org. Chem.*, 2017, **82**, 10757–10794.
- 43 T. Montagnon, M. Tofi and G. Vassilikogiannakis, *Acc. Chem. Res.*, 2008, **41**, 1001–1011.
- 44 D. Kumar, P. Sharma, H. Singh, K. Nepali, G. K. Gupta, S. K. Jain and F. Ntie-Kang, *RSC Adv.*, 2017, **7**, 36977–36999.
- 45 B. Mao, M. Fañanás-Mastral and B. L. Feringa, *Chem. Rev.*, 2017, **117**, 10502–10566.
- 46 J. A. Joule, in *Advances in Heterocyclic Chemistry*, ed. E. F. V. Scriven and C. A. Ramsden, Academic Press, 2016, vol. 119, pp. 81–106.
- 47 F. Liu, L. Anand and M. Szostak, *Chem.–Eur. J.*, 2023, **29**, e202300096.
- 48 J. A. R. Salvador, J. F. S. Carvalho, M. A. C. Neves, S. M. Silvestre, A. J. Leitão, M. M. C. Silva and M. L. Sá e Melo, *Nat. Prod. Rep.*, 2013, **30**, 324–374.
- 49 S. Wang, G. Dong and C. Sheng, *Chem. Rev.*, 2019, **119**, 4180–4220.
- 50 A. L. Harvey, R. Edrada-Ebel and R. J. Quinn, *Nat. Rev. Drug Discovery*, 2015, **14**, 111–129.
- 51 T. Liu, J. Huang, T. Liao, R. Pu, S. Liu and Y. Peng, *IRBM*, 2022, **43**, 62–74.
- 52 Z. Liu, L. Lin, Q. Jia, Z. Cheng, Y. Jiang, Y. Guo and J. Ma, *J. Chem. Inf. Model.*, 2021, **61**, 1066–1082.
- 53 X. Qian, B. Ju, P. Shen, K. Yang, L. Li and Q. Liu, *ACS Omega*, 2024, **9**, 23940–23948.
- 54 Q. Xu, A. K. X. Tan, L. Guo, Y. H. Lim, D. W. P. Tay and S. J. Ang, *Curated LOTUS database*, figshare, 2024, DOI: [10.6084/m9.figshare.25745325.v1](https://doi.org/10.6084/m9.figshare.25745325.v1).
- 55 Q. Xu, A. K. X. Tan, L. Guo, Y. H. Lim, D. W. P. Tay and S. J. Ang, *LOTUS fingerprints*, figshare, 2024, DOI: [10.6084/m9.figshare.25745448](https://doi.org/10.6084/m9.figshare.25745448).
- 56 Q. Xu, A. K. X. Tan, L. Guo, Y. H. Lim, D. W. P. Tay and S. J. Ang, *NP Atlas fingerprints*, figshare, 2024, DOI: [10.6084/m9.figshare.25745421](https://doi.org/10.6084/m9.figshare.25745421).
- 57 Q. Xu, A. K. X. Tan, L. Guo, Y. H. Lim, D. W. P. Tay and S. J. Ang, *NP Taxonomy Classification Model (MPN/SVM)*, figshare, 2024, DOI: [10.6084/m9.figshare.25745634](https://doi.org/10.6084/m9.figshare.25745634).
- 58 Q. Xu, A. K. X. Tan, L. Guo, Y. H. Lim, D. W. P. Tay and S. J. Ang, *NP Taxonomy Classification Model (Last_FFN/SVM)*, figshare, 2024, DOI: [10.6084/m9.figshare.25745598](https://doi.org/10.6084/m9.figshare.25745598).

